

On the 90th Anniversary of the Russian Academy of Sciences'  
Frumkin Institute of Physical Chemistry and Electrochemistry

## Features of Gas, Vapor, and Liquid Adsorption by Microporous Adsorbents

A. A. Fomkin<sup>a,\*</sup> and G. A. Petukhova<sup>a</sup>

<sup>a</sup>Frumkin Institute of Physical Chemistry and Electrochemistry, Russian Academy of Sciences, Moscow, 119071 Russia

\*e-mail: fomkinaa@mail.ru

Received June 14, 2019; revised August 8, 2019; accepted September 3, 2019

**Abstract**—Main features of the adsorption of gases, vapors, and liquids in microporous adsorbents, adsorption deformation, and adsorption thermodynamics are considered. Data is presented from calculating gas adsorption on microporous adsorbents in the supercritical range of temperatures using molecular dynamics and the theory of volume filling of micropores. It is shown that an adsorbate in micropores undergoes no extreme changes upon transitioning through a region of the gas phase critical state. In the adsorption of gases and vapors, the adsorption deformation of a rigid adsorbent is found to be no higher than 1% and is considerably governed by the surface chemistry and porous structure of the adsorbent.

**Keywords:** adsorption, adsorption thermodynamics, adsorption deformation, numerical modeling

**DOI:** 10.1134/S0036024420030097

### INTRODUCTION

Regardless of their chemical composition, microporous adsorbents constitute a specific class of porous solids on which physical adsorption considerably alters the properties of an adsorbed substance. The main physicochemical properties of these systems were formulated for the first time in the theory of volume filling of micropores (TVFM) [1] developed by Dubinin and his followers. In such pores, a substance is entirely within the overlapping fields of adsorption of opposite micropore walls. Its properties therefore differ substantially from those of a substance in the equilibrium bulk phase. According to Dubinin's classification [2], the effective sizes of micropores are comparable to those of the molecules to be sorbed. The range of sizes  $X$  (diameters or widths) of micropores spreads over *ultramicropores* (true micropores,  $X < 1.2$ – $1.4$  nm) and *supermicropores* ( $1.2$ – $1.4 < X < 3.0$ – $3.2$  nm). Pores with effective sizes in the range of  $3.0$ – $3.2 < X < 100$ – $200$  nm are considered *mesopores*. Adsorption in mesopores proceeds through a mechanism of layer-by-layer filling to result in capillary condensation. The sizes of mesopores are much larger than those of the adsorbed molecules. They are intermediate between micropores and *macropores* with sizes of more than  $100$ – $200$  nm. Adsorption in macropores also proceeds through a mechanism of layer-by-layer surface filling. Macropores have a considerable

effect on the kinetics of a process and, like mesopores, act as transport pores for adsorbed molecules. Similar principles are also taken as the basis for the IUPAC classification of pores by sizes [3].

Potential barriers at the entry to micropores largely shield the effects of equilibrium phase and molecules of adjacent cavities on adsorbed molecules in pores. The field of a microporous adsorbent's adsorption imposes its own structure upon the adsorbed substance and strongly disperses it. For example, each cavity of active carbon or zeolite contains from several to several dozen molecules [1, 4]. These features of a microporous system dramatically alter the properties of a substance in an adsorbed state.

During adsorption, microporous adsorbents are not just inert carriers of the adsorption field. They are also actively involved in adsorption interaction [5]. Outwardly, this manifests in deformation of the adsorbent and a change in its elastoplastic properties, depending on the  $a$ ,  $p$ ,  $T$  parameters of state of the adsorption system.

Extending adsorption processes to the high-pressure region results in the development of adsorption thermodynamics, which allows not only for the non-ideality of an equilibrium phase but the activity of an adsorbent as well [6, 7]. Analysis of the behavior of the thermodynamic functions of adsorption depending on the  $a$ – $p$ – $T$  parameters of a system allows us to draw

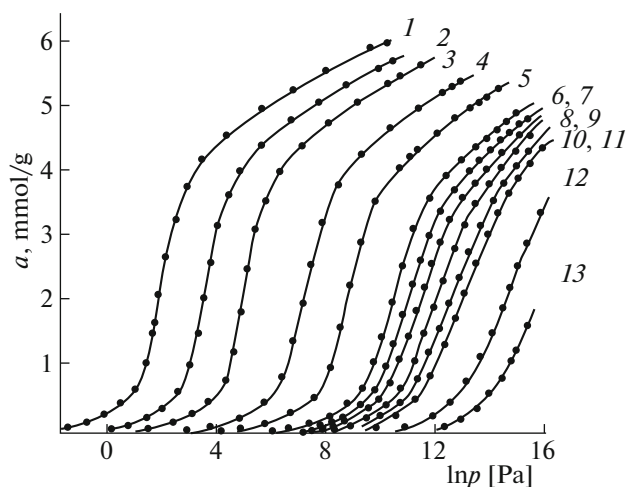


**Fig. 1.** Adsorption isotherms of Xe on the NaX zeolite at different temperatures: (1) 150, (2) 165, (3) 180, (4) 210, (5) 240, (6) 280, (7) 296, (8) 310, (9) 330, (10) 350, (11) 370, (12) 500, and (13) 600 K.

conclusions on the state and structure of an adsorbed substance in micropores. The porous structure of a solid has a key effect on the adsorption of gases, vapors, and liquids. Real adsorbents typically have a more or less wide pore size distributions [8–10].

The properties of microporous adsorbent–adsorbate adsorption systems are most pronounced in the behavior of adsorption isotherms and isosteres and the adsorption deformation of an adsorbent, along with the behavior of the thermodynamic functions of adsorption systems and their dependence on the  $a$ – $p$ – $T$  parameters of state.

#### *Adsorption of Gases and Vapors on Microporous Adsorbents*

Adsorbents with developed microporous structures and high adsorption activity are most commonly used in industry [8, 10]. Adsorbents of this type include most zeolites, along with microporous carbon adsorbents and silica gels. In zeolites, micropores are produced during the formation of their crystal structure [4]. Microporous carbon adsorbents with narrow pore size distributions are produced at quite low degrees of carbonization burning out [9]. Studies of the adsorption of gases, vapors, and liquids for a wide range of substances of different natures (e.g., Xe, Kr, Ar, N<sub>2</sub>, O<sub>2</sub>, H<sub>2</sub>, CH<sub>4</sub>, CO<sub>2</sub>, CF<sub>3</sub>Cl, *n*-C<sub>4</sub>H<sub>10</sub>, *n*-C<sub>5</sub>H<sub>12</sub>, *n*-C<sub>7</sub>H<sub>16</sub>, *n*-C<sub>9</sub>H<sub>20</sub>, H<sub>2</sub>O, C<sub>6</sub>H<sub>6</sub>, and C<sub>2</sub>H<sub>5</sub>OH) in the 0.1 Pa to 150 MPa range of pressures and the temperature range of 77 to 600 K on adsorbents with narrow pore size distributions (e.g., NaX and NaA zeolites and PAU-10 and AUK microporous adsorbents) show [4, 8, 11] that for all systems, adsorption is reversible and grows along with pressure.

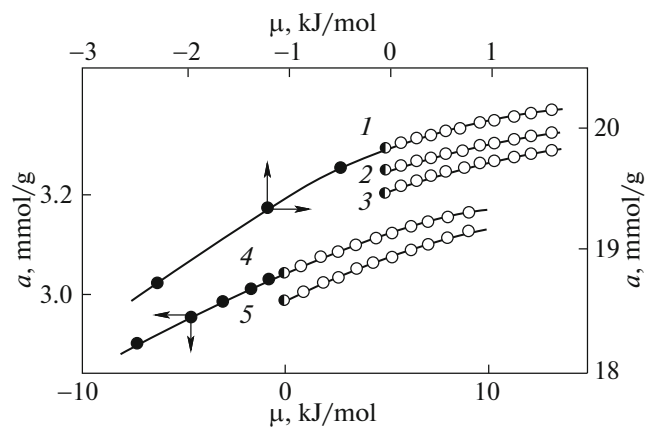


**Fig. 2.** Adsorption isotherms of (1–3) water and (4, 5) benzene on the NaX zeolite at different temperatures: (1) 303, (2) 313, (3) 323, (4) 303, and (5) 323 K;  $\mu$  is the chemical potential of the equilibrium phase. The black dots correspond to vapor adsorption; the partially filled dots, to adsorption at the line of saturated vapor pressure; and the white dots, to the adsorption of liquid at pressures of up to 100 MPa.

As an example, Figs. 1 and 2 show the adsorption isotherms of Xe, H<sub>2</sub>O, and C<sub>6</sub>H<sub>6</sub> on NaX zeolite with a micropore volume of  $W_o = 0.323$  cm<sup>3</sup>/g and an  $\alpha$ -cavity radius of  $x = 0.62$  nm [12]. Similar plots of gas adsorption versus pressure were also obtained during adsorption on microporous active carbons. As follows from Fig. 1, the adsorption isotherms shift to the high-pressure region in an almost symbate manner. They remain virtually unchanged upon going through the critical temperature of Xe ( $T_c = 289.7$  K), suggesting there were no condensation effects in the adsorbate. Similar dependences were observed for other adsorption systems as well [13–22].

No matter which state an adsorbate is in, chemical potentials  $\mu$  of the adsorptive and the adsorbate in micropores equal each other. This means adsorption isotherm  $a = f(\mu)_T$  should be unique not only upon the adsorption of a gas, but also upon adsorption of a vapor or a liquid. The adsorption isotherms of H<sub>2</sub>O and C<sub>6</sub>H<sub>6</sub> on NaX zeolite [23] shown in Fig. 2 in the  $a$ – $\mu$  coordinates were obtained by combining data on the adsorption of a vapor, a liquid under the pressure of its own saturated vapor, and a liquid under high hydrostatic pressure (up to 100 MPa).

The chemical potential of a compressed liquid under hydrostatic pressure  $P$  was calculated with the equation

$$\mu(P) = \mu(P_s^0) + \int_{P_s^0}^P v(P) dP, \quad (1)$$

where  $P_s^0$  is the saturated vapor pressure of a liquid under excess hydrostatic pressure equal to zero and  $v(P)$  is the specific volume of a compressed liquid.

The chemical potential of saturated vapor under excess hydrostatic pressure was set equal to zero, and ( $\mu(P_s^0)$ ) was taken as a zero datum at specified temperature).

As follows from Fig. 2, the adsorption isotherms in microporous adsorbents do not change their slopes upon transitioning from the region of vapor to that of a compressed liquid through the saturated vapor pressure line. The absence of jumps on the adsorption isotherms, even in the region of the isotherm's transition to the region of equilibrium phase liquid state, suggests there are no first-order phase transitions in microporous adsorbents. The number of sorbing cavities in zeolite [4] and active carbons [24, 25] were estimated to be  $\sim 10^{20}$ – $10^{21}$  per gram of adsorbent. The fine particle size of an adsorbed substance when each adsorbent cavity can contain on average up to several dozen molecules interferes with the formation of nucleating seeds of a new phase.

In the thermodynamics of adsorption, adsorption isosteres (plots of the equilibrium phase pressure as a function of temperature at a constant value of adsorption) are of great concern. It was noted in [4, 11, 26, 27] that the adsorption isosteres in the  $\ln p$ – $T^{-1}$  coordinates remain linear to a good approximation in wide ranges of pressure and temperature. Figure 3 shows the adsorption isosteres of Xe on the NaX zeolite as examples.

It follows from Fig. 3 that the adsorption isosteres of Xe remain linear throughout the range of pressures and do not change upon transitioning through the critical temperature of the equilibrium phase. At high fillings of the micropore volume, the adsorption isosteres starting in the region of vapor adsorption continue linearly in the supercritical region. Figure 3 shows the run of isosteres as a dashed line in the region where the equilibrium phase is compressed liquid xenon. The possibility of such a run of adsorption isosteres was confirmed by studying water and benzene adsorption in NaX zeolite at hydrostatic pressures of up to 100 MPa [23].

#### *Description of Adsorption Equilibria Based on the Theory of Volume Filling of Micropores*

The use of the theory of volume filling of micropores (TVFM) to describe adsorption equilibria based on the structure/energy characteristics of an adsorbent and the physicochemical parameters of adsorbed substances is well known. The theory also allows us to determine the structure/energy characteristics of an adsorbent via the adsorption of standard benzene vapor: the specific volume of micropores  $W_o$ , the effective half-width  $x$  for slit-shaped pores or the pore radius for the cylindrical pore model, and the standard characteristic energy of adsorption  $E_o$ . The Dubinin–

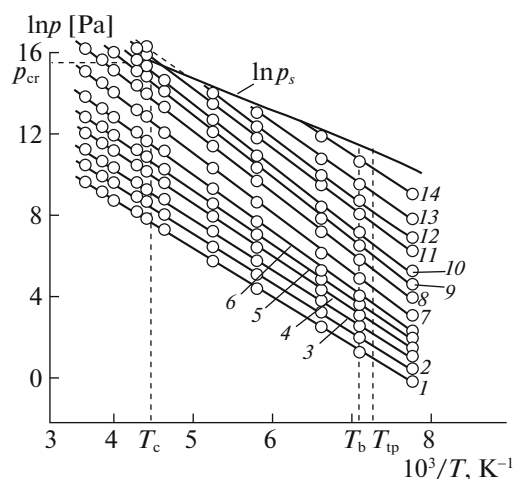


**Fig. 3.** Adsorption isosteres of Xe on the NaX zeolite at different values of adsorption: (1) 0.1, (2) 0.2, (3) 0.4, (4) 1.0, (5) 2.5, (6) 3.5, (7) 4.0, (8) 4.5, (9) 4.7, (10) 4.9, (11) 5.15, (12) 5.3, (13) 5.5, and (14) 5.8 mmol/g.  $\ln p_s$  is the line of saturated vapor pressure;  $p_c$ ,  $T_c$ ,  $T_b$ , and  $T_{tp}$  are the critical pressure, critical temperature, boiling point, and triple point temperature of xenon, respectively.

Radushkevich equation has gained widespread acceptance as the thermal equation of adsorption:

$$a = a_o(T) \exp[-(A/E)^2], \quad (2)$$

where  $a$  is adsorption determined as the total content of an adsorbate in micropores;  $a_o(T)$  is the limit adsorption of certain substance at pressure  $p$  equal to the saturated vapor pressure  $p_s$ ;  $A$  is the differential molar work of adsorption; and  $E$  is the characteristic energy of adsorption of vapor of a certain substance. Generally, the constant in the power exponent may be not be equal to two. When this is true, the equation is referred to as the Dubinin–Astakhov equation [1].

In the range of temperatures from boiling point  $T_b$  to triple point temperature  $T_{tp}$  on the line of saturation, density  $\rho_{ad}$  of the adsorbate is considered to be equal to density  $\rho_l$  of the liquid. Therefore,  $a_o(T) = W_o \rho_l$ . For higher temperatures (from  $T_b$  up to critical  $T_c$ ), the temperature dependence of limit adsorption is calculated according to Dubinin and Nikolaev [1]:

$$a_o(T) = a_o(T_b) \exp[-\alpha(T - T_b)], \quad (3)$$

where  $a_o(T_b)$  is the limit adsorption at the boiling point;  $\alpha = -(d \ln a_o / dT)_{ps}$  is the thermal coefficient of limit adsorption, determined using the  $p, T$  parameters of critical point and constant  $b$  of the Van der Waals equation for a given substance.

Differential molar work of adsorption is determined as

$$A = RT \ln(f_s/f), \quad (4)$$

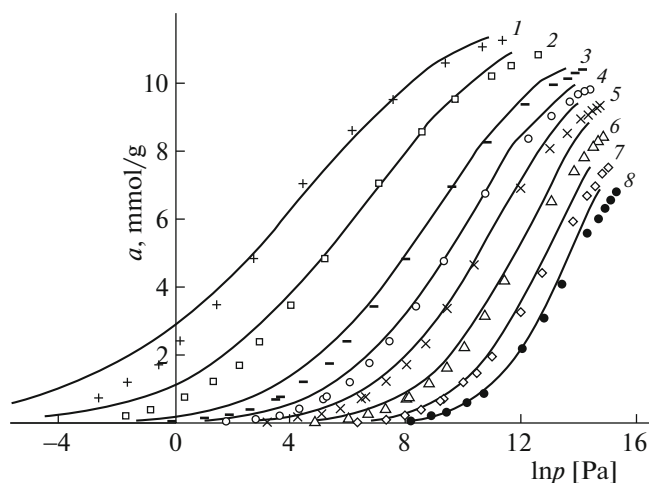


**Fig. 4.** Adsorption isotherms of  $\text{CH}_4$  on the PAU-10 microporous carbon adsorbent at different temperatures: (1) 120, (2) 140, (3) 170, (4) 190, (5) 210, (6) 240, (7) 273, and (8) 303 K. The solid lines represent calculated data based on the TVFM using the Dubinin–Radushkevich thermal equation; the symbols, experimental data.

where  $R$  is the gas constant,  $f_s$  is the saturated vapor volatility of a given substance, and  $f$  is the equilibrium phase volatility.

In Eq. (1), the characteristic energy of adsorption of a given substance is determined as  $E = \beta E_o$ , where  $\beta = P/P_o$  is the coefficient of affinity determined by the ratio of parachors  $P$  of the studied vapor and standard benzene vapor  $P_o$  at the boiling point. In the TVFM, the relationship between the effective half-width  $x_0$  of micropores, and standard characteristic energy  $E_o$  of benzene adsorption is taken as  $x_0 = 12/E_o$  based on X-ray studies of microporous carbon adsorbents.

The use of the TVFM in the region of supercritical temperature is usually limited to the range spreading by 100–150 K above the critical temperature. In this region, standard conditions pressure  $p_s$  and limit adsorption  $a_o$  are determined via linear extrapolation of (a) the saturated vapor pressure curve to the supercritical region in the  $\ln p_s - T^{-1}$  coordinates and (b) the limit adsorption curve in coordinates  $\ln a_o - T$  using Eq. (2) [1]. Similar approaches have also been used in other works [28, 29]. Such approaches have natural limitations caused by the attribution of standard  $p_s$  and  $a_o$  states at above-critical temperatures.

Another approach was used in [30]. In the range of temperatures above critical, the adsorption isotherms of gases were calculated via extrapolation based on the assumption of isostere linearity. The reference adsorption isotherms for boiling points  $T_b$  and critical temperature  $T_c$  were calculated according to the TVFM. The advantage of using the linearity of adsorption isosteres at temperatures below and above critical is

due not only to experimental findings, but to the similarity between adsorption isosteres calculated with the TVFM in the temperature range of  $T_b \leq T \leq T_c$  as well. The nonlinearity of isosteres is  $\sim 10^{-3} \text{ 1/K}$  [31]. Based on this procedure, the adsorption isotherms of  $\text{CH}_4$ , Xe, Kr, Ar,  $\text{CO}_2$ ,  $\text{N}_2$ ,  $\text{O}_2$ , and other gases were calculated to a good approximation. As an example, Fig. 4 shows the calculated data for the adsorption of methane on PAU-10 microporous carbon adsorbent, obtained via the thermal decomposition of polyvinylidene chloride in an inert medium. PAU-10 adsorbent has a narrow pore size distribution ( $W_o = 0.47 \text{ cm}^3/\text{g}$ ;  $E_o = 30.0 \text{ kJ/mol}$ ;  $x_o = 0.80 \text{ nm}$ ). The adsorption isotherms display neither hystereses nor the rise typically associated with adsorption in mesopores when approaching  $p_s$ .

As follows from Fig. 4, calculations based on the TVFM using the Dubinin–Radushkevich equation and the linearity of isosteres adequately describe the run of experimental adsorption isotherms at pressures up to 12 MPa in the sub- and supercritical regions of temperature. The greatest deviations of the calculated values from the experimental ones are seen at low temperatures in a low filling region. This situation does not contradict the TVFM [1], since the range of applicability is in this theory limited to the micropore filling range of 0.25 to 0.95.

#### Adsorption of Quantum Gases

Studying the adsorption of quantum gases (helium, hydrogen) showed that in the low-temperature range below  $T_c$ , the change in adsorption with temperature is not governed by the patterns typical of nonquantum gases. In calculating equilibria of adsorption with the TVFM, this manifested in that the temperature coefficient of limit adsorption  $\alpha$  calculated using the Dubinin–Nikolaev approach [1] was negative for hydrogen [32]. This result was likely due to quantum effects that were noted upon the adsorption of hydrogen in the range of temperatures below 50 K [33].

For this reason, the temperature dependence of limit adsorption of hydrogen  $a_o(T)$  was determined using the correlation relationship between the differential molar isosteric heat of adsorption of the average micropore volume filling of adsorbent  $\langle q_{st} \rangle$  and the reciprocal values of thermal coefficients of limit adsorption  $\alpha = -(d \ln a_o / dT)_{ps}$ . Figure 5 shows these characteristics in the  $\langle q_{st} \rangle - (1/\alpha)$  coordinates for some systems that differ in their physicochemical properties. The solid line corresponds to a polynomial approximation.

The curve must start from zero, since the heat of adsorption equal to zero corresponds to zero energy of adsorbate–adsorbent and adsorbate–adsorbate intermolecular interactions. Therefore,  $\alpha = -(d \ln a_o / dT)_{ps} \rightarrow \infty$  and  $1/\alpha \rightarrow 0$ . Since the differen-



tial heat of hydrogen adsorption according to the data from [34, 35] is  $\sim 4$  kJ/mol, it follows from Fig. 5 that  $\alpha = 2.58 \times 10^{-3} \text{ K}^{-1}$ . Analytically, function  $\langle q_{st} \rangle = f(1/\alpha)$  is well approximated by the polynomial

$$\langle q \rangle = 58.131\alpha^{-3} - 2.237\alpha^{-2} + 2.8264\alpha^{-1}. \quad (5)$$

The adsorption of hydrogen on slit-shaped structures with plane-oriented graphenes was calculated using this approach to determine  $\alpha$ , along with the linearity of adsorption isosteres and Eq. (5) [36]. The adsorption of hydrogen on plane-oriented graphenes was calculated using the AU1:3 slit-shaped model structure, where the graphene layers were at distances of 0.34 nm as in graphite, and the surface density of carbon atoms was  $\rho_C = 0.3818 \text{ atom \AA}^{-2}$ . AU1:3 adsorbent contains pores with effective width  $X = 0.538 \text{ nm}$ , standard characteristic energy of adsorption  $E_o = 44.6 \text{ kJ/mol}^{-1}$ , and micropore volume  $W_o = 1.672 \text{ cm}^3 \text{ g}^{-1}$ .

As follows from Table 1, the adsorption indices at temperatures of up to 200 K are closest to the optimum ones for hydrogen accumulators (6.5 wt %;  $695 \text{ m}^3$  of  $\text{H}_2 \text{ m}^{-3}$ ) [37].

#### Adsorption Deformation of Microporous Adsorbents

The activity of the adsorbent manifests in the variation in the size and shape of the adsorbent upon adsorption; the adsorption deformation of adsorbents with anisotropy of volume properties is anisotropic [38]. The energy contribution from adsorption deformation can be considered through the dependence of the adsorbent volume on adsorption.

Depending on the  $a$ - $p$ - $T$  parameters of the adsorption equilibrium, the adsorption deformation of microporous adsorbents can be either positive or negative. For relatively rigid adsorbents, e.g., active carbon and zeolites, adsorption deformation is usually not higher than one percent. Until recently, little attention was given to studying adsorption deformation. However, the extension of the fields of application of adsorption processes, especially to the high-pressure region, requires the contribution of adsorption deformation to the thermodynamic characteristics of adsorption to be refined. In addition, adsorption deformation largely governs the mechanical strength and stability of an adsorbent in such fast processes as PSA, where the number of adsorption-adsorption cycles grows by more than a thousand. Until recently, insufficient attention was given to the theory of adsorption deformation. Phenomenal approaches [39–41] could not explain the details of adsorption interaction resulting in adsorption deformation or its dependences on temperature and micropore filling. In recent years, new means have emerged that are based on applying molecular statistical approaches to adsorption in micropores. In [42], the adsorption deformation of nanoporous adsorbents was

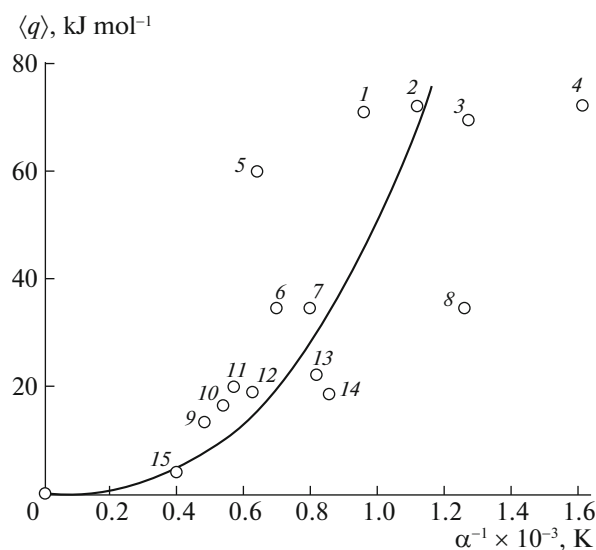


**Fig. 5.** Differential molar isosteric heat of adsorption of the mean micropore filling  $\langle q \rangle$  of different substances as a function of the reciprocal temperature coefficient of limit adsorption  $\alpha$  for different systems: (1) ( $n$ - $\text{C}_8\text{H}_{18}$ -NaX zeolite), (2) ( $\text{H}_2\text{O}$ -NaX), (3) ( $\text{C}_6\text{H}_6$ -NaX), (4) ( $n$ - $\text{C}_7\text{H}_{16}$ -NaX), (5) ( $\text{H}_2\text{O}$ -NaX), (6) ( $\text{CF}_3\text{Cl}$ -NaX), (7) ( $\text{N}_2$ -NaX), (8) ( $\text{CO}_2$ -NaX), (9) ( $\text{Ar}$ -MaX), (10) ( $\text{N}_2$ -active carbon), (11) ( $\text{Kr}$ -NaX), (12) ( $\text{CH}_4$ -PAU-10 active carbon), (13) ( $\text{Xe}$ -NaX), (14) ( $\text{CH}_4$ -NaX), and (15) the point corresponding to the adsorption of hydrogen. Our approximation is shown as the solid line.

explained using the statistical mechanical theory of the molecular structure of surface layers. The observed effects of the adsorption compression of adsorbents were shown to result from the anisotropy of the pressure tensor of an adsorbate in micropores. The density functional theory [43] and molecular statistical approaches [44] were used in other works. Nevertheless, the theory of adsorption deformation of solids is still at the initial stage of development.

The dependences of adsorption deformation on the magnitude of adsorption and temperature can have regions of compression and expansion. Figure 6 shows the dependences of the relative linear adsorption deformation of the AUK microporous carbon adsor-

**Table 1.** Adsorption of hydrogen ( $a$ ) on the model AU1:3 adsorbent at a pressure of 20 MPa, calculated with the TVFM

$T, \text{ K}$	77	200	300	400
$a, \text{ mmol g}^{-1}$	55	42	23	8
$d, \text{ wt \%}$	11.0	8.4	4.6	1.6
$d_v$	583	445	244	85

$d$  is the  $\text{H}_2$  gravimetric density,  $d_v$  is the volume density of  $\text{H}_2$ ,  $\text{m}^3$  of  $\text{H}_2$  at NTP (cubic meters of hydrogen at normal temperature and pressure (293 K, 101 kPa) per storage system volume,  $\text{m}^3$ ).

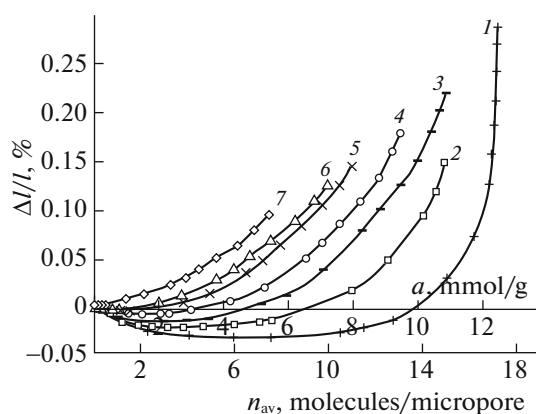


**Fig. 6.** Adsorption-induced deformation of the AUK microporous carbon adsorbent as a function of the  $\text{CH}_4$  adsorption and the average number of methane molecules in single micropore at different temperatures: (1) 177.65, (2) 216.2, (3) 243.3, (4) 273.15, (5) 313, (6) 333, and (7) 393 K. The symbols correspond to experimental data; the lines, to approximation.

bent on the adsorption of methane in the supercritical temperature range of 243–393 K at pressures of up to  $\sim 10$  MPa.

As follows from Fig. 6, the curves of adsorption-induced deformation of the adsorbent upon the adsorption of methane on the AUK active carbon have a region of compression only at relatively low temperatures (177.65–313 K). The highest adsorption-induced expansive deformation of the adsorbent is  $\sim 0.3\%$ , and the compressive deformation does not exceed  $0.03\%$ . There is no region of compression in the range of higher temperatures (313–393 K). Compression of a solid is associated with the forces of interaction between adsorbed  $\text{CH}_4$  molecules and the opposite micropore walls. The diameter of methane molecules (0.42 nm) is in this case comparable to the effective pore width of the AUK adsorbent (0.82 nm). Upon an increase in the micropore volume filling, however, the average distance between adsorbed  $\text{CH}_4$  molecules, and the average distance between the molecules and the pore walls, shrink and the forces of repulsion grow, resulting in considerable expansion of the AUK adsorbent. At 177.65 K and 6 MPa, the maximum expansion of the AUK adsorbent is around ten times higher than the initial compression.

Upon an increase in temperature, the region of adsorbent initial compression gradually contracts and disappears at  $\sim 333$  K. At 393 K, a dramatic expansion of the adsorbent up to  $0.002\%$  is observed at the beginning of the isotherm, followed by a smooth increase with an increase in the adsorption of  $\text{CH}_4$ . Similar dependences were also obtained upon the adsorption of  $\text{CO}_2$ , Ar, Xe, Kr,  $\text{CH}_4$ ,  $\text{N}_2$ , and  $\text{O}_2$ .

The initial expansion of the AUK adsorbent was due not only to an increase in the kinetic energy of

adsorbed molecules, since the adsorption values are low and the differential heat of  $\text{CH}_4$  adsorption is quite high ( $\sim 22$  kJ/mol). This behavior of adsorption deformation was likely due to the anisotropy of the elastic properties of the carbon adsorbent being associated with temperature, and especially to the weakening of bonds between hexagonal carbon layers in the walls of slit-shaped adsorbent pores with a temperature increase. As a result, the first molecules entering a pore constrict the neighboring carbon layers, unbalancing the forces in the solid and increasing the distance between the following layers. From a macroscopic perspective, this results in expansion of the solid. The subsequent expansion of the adsorbent with an increase in adsorption was likely due to a change in the balance of forces associated with an increase in the inner pressure of adsorbate upon a rise in micropore adsorption and the compressibility of porous solid along with temperature.

The adsorption of molecules with effective sizes close to those of an adsorbent has unique features. The adsorption deformation of the AUK adsorbent upon the adsorption of *n*-pentane, *n*-heptane, and *n*-octane was studied at temperatures of 243.3, 273.15, 293, 313, 353, and 393 K. As an example, Fig. 7 shows typical dependences of the relative linear deformation of the AUK adsorbent on the adsorption value for *n*-pentane. As follows from Fig. 7, there is almost no adsorption deformation of the AUK in the initial region of micropore filling. For the lowest temperature of 243.3 K upon adsorption of 4.8 mmol/g, there is a slight region of compression to  $0.01\%$ , after which the adsorption deformation moves to the region of expansion and rapidly grows to  $0.7\%$  upon adsorption of 5.4 mmol/g. At higher temperatures, the adsorption deformation moves to the region of expansion at lower adsorption values.

This behavior of the deformation curves was likely due to steric relations and the specificity of interaction between molecules and the micropore wall surface. The energy of interaction between the molecules and pore walls is minimal in the region of the initial filling, and the force is close to zero of the close sizes of molecules and micropores. Upon an increase in the micropore filling, forces of repulsion between all participants of interaction increase and the adsorbent expands. The effect of steric factors upon adsorption is especially visible in the delayed kinetics of adsorption. The time required for equilibration at low pressures was as long as 5–8 h.

#### *Energetics of Adsorption*

The energetics of adsorption of gases and vapors in microporous adsorbents differs greatly from adsorption on the open surface of a nonporous solid. In the former case, adsorption occurs through the mechanism of bulk micropore filling; in the latter, the adsorbate forms a separate phase on the solid surface.

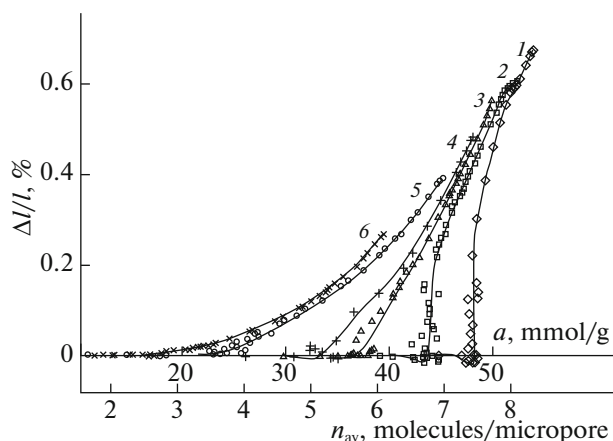


**Fig. 7.** Adsorption-induced deformation of the AUK microporous carbon adsorbent as a function of  $n$ -C<sub>5</sub>H<sub>12</sub> adsorption and the average number of  $n$ -pentane molecules in single micropore at different temperatures: (1) 243.3, (2) 273.15, (3) 293, (4) 313, (5) 353, and (6) 393 K. The symbols correspond to experimental data; the lines, to fitting curves.

Determining the volume of a solid body with micropores is generally a quite complex problem. For crystalline zeolites, this can be done using data from X-ray diffraction and chemical analysis [4]. This problem for entirely microporous adsorbents was solved in [45]. The adsorption determined in this manner is the total content, rather than the excess, in the micropore volume (absolute adsorption).

By definition, the differential isosteric heat of adsorption is the difference between the molar enthalpy of gas phase  $h_g$  and the differential enthalpy of adsorption system  $h_1 = (dH_1/da)_T$ :

$$q_{st} = h_g - (dH_1/dN_a)_T = h_g - h_1. \quad (6)$$

It was shown in [6, 7] that the differential isosteric heat of adsorption can be calculated from the equilibrium adsorption and deformation data using the equation

$$q_{st} = -Rz(d \ln P/dT^{-1})_a [1 - (dv_1/da)_T/V_g] - (dP/da)_T [v_1 - T(dv_1/dT)_a], \quad (7)$$

where  $z = pv_g/RT$  is the compressibility factor of the gas phase at pressure  $p$ , temperature  $T$ , and gas phase specific volume  $v_g$ ;  $R$  is the gas constant;  $v$  is the specific reduced volume of the adsorbent–adsorbate system, calculated relative to the weight of the regenerated adsorbent; and  $a$  is adsorption, determined as the total content of the substance in micropores.

If pressures are low,  $z = 1$ , and the adsorbent is not deformed upon adsorption  $v_1 \neq v_1(a, T)$ , then

$$q_{st} = -R(d \ln p/dT^{-1})_a + v_1(dP/da)_T. \quad (8)$$

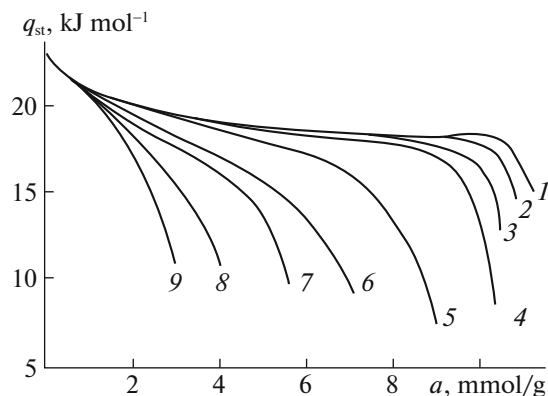


**Fig. 8.** Differential molar isosteric heat of CH<sub>4</sub> adsorption on the PAU-10 microporous adsorbent as a function of adsorption at different temperatures: (1) 120, (2) 150, (3) 170, (4) 190, (5) 273, (6) 370, (7) 410, (8) 500, and (9) 600 K.

In the low-pressure region ( $p < 100$  kPa), the last member is usually small, so we obtain a typical equation for the differential heat of adsorption:

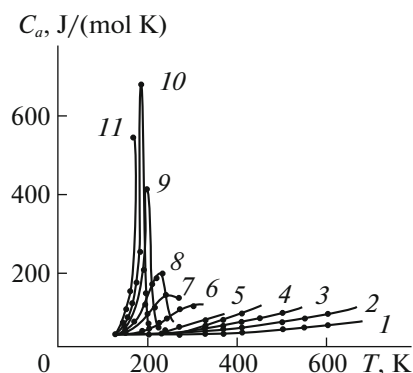
$$q_{st} = -R(d \ln P/dT^{-1})_a. \quad (9)$$

Figure 8 shows the plots of differential molar isosteric heat of methane adsorption versus the value of adsorption on PAU-10 microporous adsorbent at pressures of up to 12 MPa. As follows from Fig. 6, considering all corrections in accordance with Eq. (7) resulted in the heat of adsorption depending largely on the temperature. The nonideality of the gas phase and the adsorption deformation of the adsorbent have almost no effect on the heat of adsorption at 120 K. In the region of initial micropore fillings up to 3 mmol/g, the heat of adsorption drops rapidly from 24 to 19 kJ/mol, due to the filling of the most active adsorption centers with methane molecules. Subsequent bulk filling of micropores up to 9.5 mmol/g results in a heat close to ~18–19 kJ/mol. At high fillings (~10 mmol/g), the adsorption heat curve displays a weakly pronounced maximum (~20 kJ/mol) and then a dramatic drop of up to ~15 kJ/mol at adsorption of ~11.5 mmol/g.

The maximum on the curve of the heat of CH<sub>4</sub> adsorption on PAU-10 results from an increase in the heat of adsorption due to a rise in the energy of adsorbate–adsorbate attraction, and a drop in the heat of adsorption due to a rise in the energy of repulsion at small distances. As follows from Fig. 7, considering all of the allowances in accordance with Eq. (7) results in a strong temperature dependence of the heat of adsorption.

Such effects are often observed upon the adsorption of vapors on zeolites [4].

This was confirmed in [46] by allowing for the adsorption deformation of zeolite through direct



**Fig. 9.** Differential molar isosteric heat capacity of the methane–PAU-10 microporous carbon adsorbent adsorption system as a function of temperature at different values of adsorption: (1) 1.0, (2) 3.0, (3) 4.0, (4) 5.0, (5) 6.0, (6) 8.0, (7) 9.0, (8) 9.5, (9) 10.0, (10) 10.3, and (11) 10.5 mmol/g.

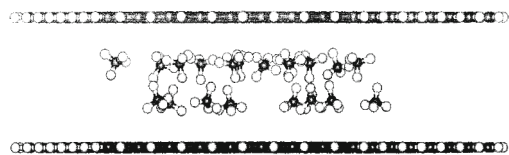


**Fig. 10.** Image of the MD trajectory of 20  $\text{CH}_4$  molecules in a slit-shaped pore with graphene walls at 273 K. The black dots are carbon atoms.

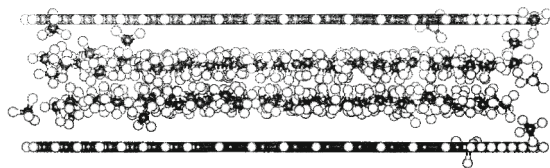


**Fig. 11.** Image of the MD trajectory of 160  $\text{CH}_4$  molecules in a slit-shaped pore with graphene walls at 273 K.

experimental calorimetric study of Xe adsorption on NaX zeolite at pressures of up to 20 MPa. On active carbons, the maxima on the adsorption heat curve are observed much more rarely, and mainly upon adsorption on the adsorbent with a narrow pore size distribution. The AUK and PAU-10 adsorbents correspond to these requirements.

Analysis of dependences of variation in the differential entropy and isosteric heat capacity of an adsorption system shows that, at high micropore fillings, adsorption associates can form thanks to the energy of attraction between adsorbed molecules. The adsorbate in micropores is so strongly dispersed that the formation of a liquid phase becomes impossible, but precursors of the phase (molecular associates) are produced. The formation of associates in micropores explains the emergence of maxima on the curves of differential

molar isosteric heat capacity of an adsorption system  $C_a$  as a function of temperature with an increase in micropore volume filling with adsorbed molecules. Figure 9 shows that with an increase in the adsorption of methane, the maxima on the heat capacity curves become ever more pronounced.

This phenomenon was confirmed via molecular dynamics modeling of an adsorption system.

#### *Numerical Modeling of Adsorption in Slit-Shaped Micropores*

In the molecular dynamics (MD) calculations in [25], atom–atom potentials as universal force fields were used with respect to adsorption in a model pore using the TINKER molecular dynamics program package [47] with the OPLS-AA [48] and MM3 [49] force fields. A micropore in the form of a washer with open side walls was taken as a model. The adsorbing surfaces were graphene single-layer planes. The micropore model with a diameter of 38.8 nm and slit width  $d = 0.82$  nm (the distance between the centers of carbon atoms forming adsorbing surfaces) was placed in the center of program-specified cell in the form of parallelepiped with dimensions of  $8 \times 8 \times d$  nm and periodic boundary conditions. The space beyond the micropore simulated the bulk phase. During a numerical experiment, the adsorbate molecules could be in the adsorption, surface, or vapor phases. A given number of molecules was placed in this system at a constant temperature and their trajectories were calculated.

Figures 10 and 11 show the MD modeling data for the adsorption of methane in the model micropore at fillings of 0.1 and 0.9 of the maximum one. As follows from these figures, the association of methane occurs in the central portion of pore. Most of the adsorbed molecules are in the associate. With an increase in filling, the methane associates increase. It is characteristic that the structure of associates has two layers. The layers are in parallel with the graphene planes.

The adsorption isotherms of methane (in a wide range of temperatures below and above the critical value), ethane, propane, butane, ethylene, propylene, benzene, and ethanol were calculated, along with the isotherms of components of a benzene–ethanol liquid mixture and a propane–butane gas mixture. The molecular nanostructures of adsorbed methane, benzene, and ethanol were analyzed, and the concentration and isomeric composition of associates of adsorbed and liquid ethanol were calculated [50, 51].

## CONCLUSIONS

Microporous adsorbents are a specific class of porous solids in which physical adsorption alters the properties of an adsorbed substance considerably. The substance is entirely within the overlapping adsorption fields of opposite micropore walls. Its properties



therefore differ greatly from those of a substance in the equilibrium bulk phase. The adsorption field of a microporous adsorbent imposes its structure upon an adsorbed substance and strongly disperses it. Adsorbents are actively involved in the adsorption interaction. Outwardly, this manifests in the deformation of the adsorbent and a change in its elastoplastic properties, depending on the  $a-p-T$  parameters of state of the adsorption system. The properties of microporous adsorbent–adsorbate adsorption systems are most pronounced in the behavior of adsorption isotherms and isosteres and the adsorption deformation of the adsorbent, and in the behavior of thermodynamic functions of adsorption systems and their dependences on the  $a-p-T$  parameters of state. Regardless of which state is adsorptive, chemical potentials  $\mu$  of the adsorptive and adsorbate in micropores are equal to each other. This means the adsorption isotherm  $a = f(\mu)_T$  must be unique not only upon gas adsorption, but also upon vapor and liquid adsorption. The absence of jumps on the adsorption isotherms, even in the region of isotherm transition to the region of equilibrium phase liquid state, suggests there are no first-order phase transitions in microporous adsorbents. In the  $\ln p-T^{-1}$  coordinates, the adsorption isosteres remain linear to a good approximation in wide ranges of pressure and temperature. At high micropore volume fillings, the adsorption isosteres starting in the region of vapor adsorption continue linearly in the supercritical region. Calculations based on the TVFM using the Dubinin–Radushkevich equation and the linearity of isosteres satisfactorily describe the form of experimental adsorption isosteres at pressures up to 12 MPa in the subcritical and supercritical temperature ranges. The extension of application fields of adsorption processes, especially to the high-pressure region, requires the contribution from adsorption deformation to the thermodynamic characteristics of adsorption to be refined. In addition, the adsorption deformation largely governs the mechanical strength and stability of an adsorbent in fast processes of gas mixture separation. The dependences of the adsorption deformation on the magnitude of adsorption and the temperature can have regions of compression and expansion. The energetics of the adsorption of gases and vapors in microporous adsorbents depend greatly on the pressure of the equilibrium phase and the adsorption deformation of the adsorbent.

Analysis of the changes in the differential entropy and isosteric heat capacity shows that at high micropore fillings, adsorption associates can form thanks to the energy of attraction between adsorbed molecules. The adsorbate in micropores is so strongly dispersed that the formation of liquid phase becomes impossible and liquid phase precursors (molecular associates) are produced. The formation of associates in micropores explains the emergence of maxima on the curves of the differential molar isosteric adsorption heat capacity  $C_a$  as a function of temperature with an increase in micro-

pore volume filling with adsorbed molecules at fillings of 0.1 and 0.9 of the highest one. The structure of adsorbed associates and the deformation of microporous adsorbent depend greatly on the energy of adsorption, the size ratio of pores and adsorbate molecules, and the degree of pore space filling.

## REFERENCES

1. M. M. Dubinin, *Adsorption and Porosity* (VAKhZ, Moscow, 1972) [in Russian].
2. M. M. Dubinin, *Izv. Akad. Nauk SSSR, Ser. Khim.*, 996 (1974).
3. D. H. Everett, *Pure Appl. Chem.* **31**, 577 (1972).
4. D. Breck, *Zeolite Molecular Sieves* (Wiley, New York, 1974).
5. B. P. Bering, A. Maiers, and V. V. Serpinskii, *Dokl. Akad. Nauk SSSR* **193**, 119 (1970).
6. V. A. Bakaev, Doctoral (Phys. Math.) Dissertation (Mosc. State Univ., Moscow, 1989).
7. A. A. Fomkin, *Adsorption* **11**, 425 (2005).
8. N. S. Polyakov and G. A. Petukhova, *Russ. Khim. Zh.* **39** (6), 7 (1995).
9. G. A. Petukhova, N. S. Polyakov, F. G. Lupashku, and L. I. Monakhova, *Russ. Chem. Bull.* **44**, 1854 (1995).
10. G. A. Petukhova, *Prot. Met. Phys. Chem. Surf.* **44**, 157 (2008).
11. M. M. Dubinin and H. F. Stoeckli, *J. Colloid Interface Sci.* **75**, 34 (1980).
12. A. A. Fomkin, V. V. Serpinskii, and K. Fidler, *Russ. Chem. Bull.* **31**, 1071 (1982).
13. A. A. Fomkin and V. V. Serpinskii, *Russ. Chem. Bull.* **23**, 2026 (1974).
14. B. P. Bering, I. I. Seliverstova, V. V. Serpinskii, and A. A. Fomkin, *Russ. Chem. Bull.* **26**, 2606 (1977).
15. E. V. Chkhaidze, A. A. Fomkin, V. V. Serpinskii, and G. V. Tsitsishvili, *Russ. Chem. Bull.* **34**, 886 (1985).
16. E. V. Chkhaidze, A. A. Fomkin, V. V. Serpinskii, et al., *Russ. Chem. Bull.* **35**, 847 (1986).
17. A. B. Kharitonov, V. A. Sinitsyn, and A. A. Fomkin, *Izv. Akad. Nauk SSSR, Ser. Khim.*, No. 6, 1018 (2000).
18. A. A. Fomkin, *Adsorption* **11**, 425 (2005).
19. A. V. Shkolin, A. A. Fomkin, and V. Yu. Yakovlev, *Russ. Chem. Bull.* **56**, 393 (2007).
20. A. A. Fomkin, *Prot. Met. Phys. Chem. Surf.* **45**, 121 (2009).
21. S. V. Potapov, A. A. Fomkin, and V. A. Sinitsyn, *Russ. Chem. Bull.* **58**, 733 (2009).
22. S. V. Potapov, A. A. Fomkin, V. A. Sinitsyn, A. V. Shkolin, and A. L. Pulin, *Prot. Met. Phys. Chem. Surf.* **46**, 519 (2010).
23. A. A. Fomkin, V. A. Avramenko, I. I. Seliverstova, and V. V. Serpinskii, *Dokl. Akad. Nauk SSSR* **288** (3), 678 (1986).
24. M. M. Dubinin, in *Carbon Adsorbents and Their Application in Industry* (Nauka, Moscow, 1983), p. 100 [in Russian].
25. A. V. Shkolin, Cand. Sci. Dissertation (Inst. Phys. Chem. Electrochem. RAS, Moscow, 2008).

26. M. Bülov, D. Shen, and S. Jale, *Appl. Surf. Sci.* **196**, 157 (2002).
27. R. M. Barrer and R. Papadopoulos, *Proc. R. Soc. London A* **326**, 315 (1972).
28. M. M. Dubinin, O. Kadlets, and V. V. Serpinskii, *Russ. Chem. Bull.* **33**, 455 (1984).
29. I. E. Ovcharenko, A. M. Tolmachev, and A. A. Fomkin, *Russ. Chem. Bull.* **42**, 1606 (1993).
30. A. A. Fomkin, E. V. Chkhaidze, V. V. Serpinskii, G. V. Tsitsishvili, and M. M. Dubinin, *Izv. Akad. Nauk SSSR, Ser. Khim.*, No. 1, 43 (1989).
31. A. V. Shkolin, A. A. Fomkin, and V. Yu. Yakovlev, *Russ. Chem. Bull.* **56**, 393 (2007).
32. A. A. Fomkin and V. A. Sinitsyn, *Prot. Met. Phys. Chem. Surf.* **44**, 150 (2008).
33. G. Stan and M. W. Cole, *J. Low Temp. Phys.* **110**, 539 (1998).
34. V. S. Kogan and K. G. Breslavets, in *Adsorption and Porosity*, Ed. by M. M. Dubinin and V. V. Serpinskii (Nauka, Moscow, 1976), p. 270 [in Russian].
35. K. G. Breslavets, V. S. Kogan, Yu. Ya. Milenko, et al., *Vopr. At. Nauki Tekh.*, No. 1 (2), 12 (1972).
36. A. A. Fomkin and V. A. Sinitsyn, *Prot. Met. Phys. Chem. Surf.* **44**, 150 (2008).
37. A. C. Dillon, K. M. Jones, T. A. Bekkedahl, et al., *Nature (London, U.K.)*, No. 386, 377 (1997).
38. A. V. Tvardovskii, A. A. Fomkin, Yu. I. Tarasevich, I. G. Polyakova, V. V. Serpinskii, and I. M. Guseva, *Russ. Chem. Bull.* **41**, 987 (1992).
39. E. A. Flood, *Can. J. Chem.* **35**, 48 (1957).
40. B. P. Bering, O. K. Krasil'nikova, and V. V. Serpinskii, *Dokl. Akad. Nauk SSSR* **231**, 373 (1976).
41. V. V. Serpinskii and T. S. Yakubov, *Russ. Chem. Bull.* **30**, 54 (1981).
42. A. I. Rusanov, *Colloid. J.* **69**, 807 (2007).
43. E. A. Ustinov and D. D. Do, *Carbon* **44**, 2652 (2006).
44. P. Kovalczyk, A. Ciach, and A. V. Neimark, *Langmuir* **24**, 6603 (2008).
45. A. A. Fomkin, I. I. Seliverstova, and V. V. Serpinskii, *Russ. Chem. Bull.* **35**, 256 (1986).
46. V. Y. Gusev and A. A. Fomkin, *Adsorption Sci. Technol.* **8** (2), 75 (1991).
47. <http://dasher.wustl.edu/tinker/>.
48. W. L. Jorgensen, D. S. Maxwell, and J. Tirado-Rives, *J. Am. Chem. Soc.* **118**, 11225 (1996).
49. N. L. Allinger, Y. H. Yuh, and J.-H. Lii, *J. Am. Chem. Soc.* **111**, 8551 (1989).
50. A. M. Tolmachev, K. M. Anuchin, N. G. Kryuchenkova, and A. A. Fomkin, *Prot. Met. Phys. Chem. Surf.* **47**, 150 (2011).
51. A. M. Tolmachev, D. A. Firsov, K. M. Anuchin, and T. A. Kuznetsova, *Prot. Met. Phys. Chem. Surf.* **45**, 163 (2009).

*Translated by K. Utegenov*